Magnetic-field dependence of the ferroelectric polarization and spin-lattice coupling in multiferroic $MnWO_4$

K. Taniguchi,[1] N. Abe,[2] H. Sagayama,[1] S. Ohtani,[2] T. Takenobu,[3] Y. Iwasa,[3] and T. Arima[1]
[1]*Institute of Multidisciplinary Research for Advanced Materials, Tohoku University, Sendai 980-8577, Japan*
[2]*Department of Physics, Tohoku University, Sendai 980-8578, Japan*
[3]*Institute for Material Research, Tohoku University, Sendai 980-8577, Japan*
(Received 1 October 2007; revised manuscript received 5 December 2007; published 8 February 2008)

The magnetic-field dependence of the ferroelectric polarization and the spin-lattice coupling in multiferroic $MnWO_4$ have been investigated. The ferroelectric transition from the low temperature paraelectric phase occurs when the magnetic field is applied along the *a*, *c*, and the spin easy axes. The ferroelectric polarization in the magnetic field along the *a* and the *c* axis shows a contrasting behavior depending on the field direction, possibly reflecting the relative configuration between the crystallographic axis and the magnetic principal axis in the *ac* plane. Incommensurate lattice modulation observed in the ferroelectric spiral-spin phase confirms the existence of spin-lattice coupling in $MnWO_4$. The lattice modulation indicates that the ferroelectric AF2 phase also takes the incommensurate magnetic structure in a magnetic field. In the high-field phase, which appears in high magnetic fields above 12 T along the easy axis, the magnetic-field-induced ferroelectric polarization disappeared.

DOI: 10.1103/PhysRevB.77.064408 PACS number(s): 75.80.+q, 64.70.Rh, 75.30.Kz

I. INTRODUCTION

In recent years, a new class of multiferroic materials, in which magnetic order induces a ferroelectric (FE) phase transition, has attracted much attention, since they often show the gigantic magnetoelectric effects.[1–11] The common feature of these materials is the FE phase appearance in the long-wavelength magnetic order phase with noncollinear spin configuration. In particular, recent neutron diffraction studies in perovskite $R\mathrm{MnO_3}$ (R=Tb, $\mathrm{Tb_{1-x}Dy_x}$)[12,13] show that the ferroelectricity arises from the cycloidal spiral-spin structure, in which the spin rotation axis is not parallel to the magnetic modulation vector. This correlation between the ferroelectricity and the cycloidal spiral-spin structure is in accord with the theory associated with the Dzialoshinski-Moriya interaction.[14–16] According to the microscopic model proposed by Katsura *et al.*,[14] the canted spin moments on two neighboring sites, $\boldsymbol{S}_i$ and $\boldsymbol{S}_j$, should induce an electric dipole moment,

$$\boldsymbol{p} = A\boldsymbol{e}_{ij} \times (\boldsymbol{S}_i \times \boldsymbol{S}_j). \quad (1)$$

Here, $\boldsymbol{e}_{ij}$ denotes the unit vector connecting the two sites. The coefficient A is a constant, which depends on the spin-orbit coupling and superexchange interaction. Equation (1) indicates that the macroscopic electric polarization can appear when a magnetic order phase takes the cycloidal spiral-spin structure. Recent studies have reported that some systems other than perovskite $R\mathrm{MnO_3}$ (R=Tb, Dy), also belong to this type of multiferroic material.[4–8]

$MnWO_4$ is one of the multiferroic materials in which the cycloidal spin structure induces ferroelectricity.[6] This material is crystallized in a wolframite structure, which belongs to the monoclinic space group $P2/c$ with $\beta \sim 91°$ at room temperature (see Fig. 1).[17] The crystal structure is characterized by alternative stacking of manganese and tungsten layers along the *a* axis [Fig. 1(a)]. As shown in Fig. 1(a), MnO_6 and WO_6 octahedra are aligned in zigzag chains along the *c* axis. $MnWO_4$ is known as a frustrated magnet with only one kind of magnetic ion, Mn^{2+} (S=5/2). The ratio of the Weiss temperature (θ) to the Néel temperature (T_N) is reported to be 5–6,[6,18,19] indicating that the magnetic interactions are moderately frustrated in this system. While other wolframites $M\mathrm{WO_4}$ (M=Fe, Co, Ni) show only one magnetic transition to the commensurate magnetic (CM) state with a propagation vector $\boldsymbol{k}$=(1/2,0,0), $MnWO_4$ undergoes successive magnetic phase transitions at ~13.5 K (T_N), ~12.7 K (T_2), and ~7.5 K (T_1), related to three long-wavelength magnetic or-

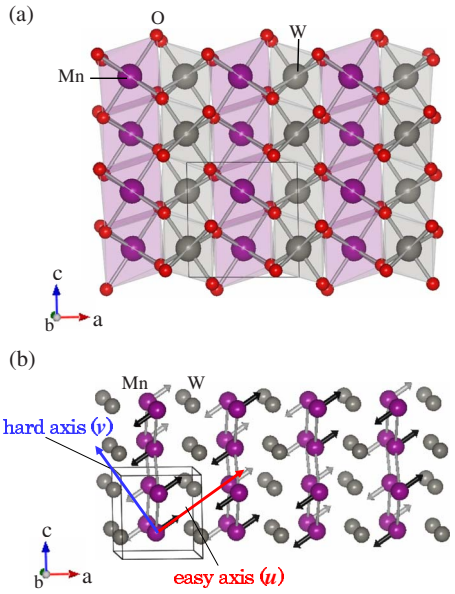

FIG. 1. (Color online) (a) Crystal structure of $MnWO_4$ viewed along the *b* axis: each cation [Mn: purple (dark gray); W: gray] is surrounded by an oxygen [red (dark gray) small sphere] octahedron. (b) Collinear magnetic structure in AF1: magnetic moments lie in the *ac* plane and cant to the *a* axis by ~35°. The magnetic principal axes in the *ac* plane, which are the easy and hard axes, are also displayed.

dering states, AF3, AF2, and AF1.[20] According to neutron diffraction results,[20] AF1 ($T<T_1$), AF2 ($T_1<T<T_2$), and AF3 ($T_2<T<T_N$) are a commensurate (C) collinear antiferromagnetic (AFM) phase, an incommensurate (IC) elliptical-spiral phase, and an IC-collinear AFM phase, respectively. The respective propagation vectors are $\boldsymbol{k}=(\pm 1/4,1/2,1/2)$ for AF1 and $\boldsymbol{k}=(-0.214,1/2,0.457)$ for AF2 and AF3. In AF1 and AF3, magnetic moments collinearly align in the *ac* plane, forming an angle of about 35° with the *a* axis [Fig. 1(b)], whereas in AF2, an additional component in the [010] direction exists.[20] Therefore, the magnetic principal axis setting, which is the orthogonal one, is different from the crystallographic monoclinic setting. In this study, we define the magnetic principal axes within the *ac* plane as the easy and the hard axis, respectively, as shown in Fig. 1(b). In this definition, the easy axis ($\boldsymbol{u}$) is parallel to the spin-aligned direction within the *ac* plane, and the hard axis ($\boldsymbol{v}$) is perpendicular both to the easy axis and to the *b* axis.

In the present study, we have investigated the correlation between the FE polarization and the spin order in $MnWO_4$ in magnetic fields through synchrotron radiation diffraction and the electric-polarization measurements. $MnWO_4$ is the prototype system for the investigation of the magnetic-field effect on the spiral-spin-induced FE phase, since $MnWO_4$ contains only one kind of magnetic ion, Mn^{2+}, and has a simple crystal structure with only one crystallographic site. We have observed a FE phase transition induced by the application of a magnetic field (H) along the easy axis. The induced FE polarization disappears again in the high-field (HF) phase above 12 T. We have found that the FE phase transition is also induced by the magnetic field parallel to the *a* or the *c* axis. This fact indicates that the easy axis component of a magnetic field, which stabilizes the FE AF2 phase, is more dominant than the hard axis one in the *ac* plane. The C-IC change of the lattice modulation vector has been confirmed simultaneously. The magnetic field has induced phase transition from AF1 to AF2 phase. We have also observed that the magnetic-field dependence of the FE polarization in $H\|a$ is different from that in $H\|c$.

II. EXPERIMENT

Polycrystalline rods of $MnWO_4$ were synthesized by a conventional solid-state reaction at 1000 °C in air starting from MnO and WO_3. Single crystals were grown by the floating-zone method in airflow with a feed speed of 3 mm/h. A typical size of single crystals was 5 mm ϕ $\times$4 cm. The resulting crystals appear to be blood red and transparent in the thin section. They were oriented using Laue x-ray photographs and cleaved into thin plates with the widest faces perpendicular to the crystallographic principal axis *b*. Off-resonant single crystal x-ray diffraction measurements were performed on beam line 3A at Photon Factory, Japan. X-ray beams monochromated to 14 keV by utilizing a Si (111) double-crystal monochromator were focused on a (010) surface of the sample in a He-flow cryostat equipped with a superconducting magnet. The superlattice reflections were surveyed in the reciprocal space of $(h,-5,l)$ in a magnetic field applied along the *c* axis. For the measurement of

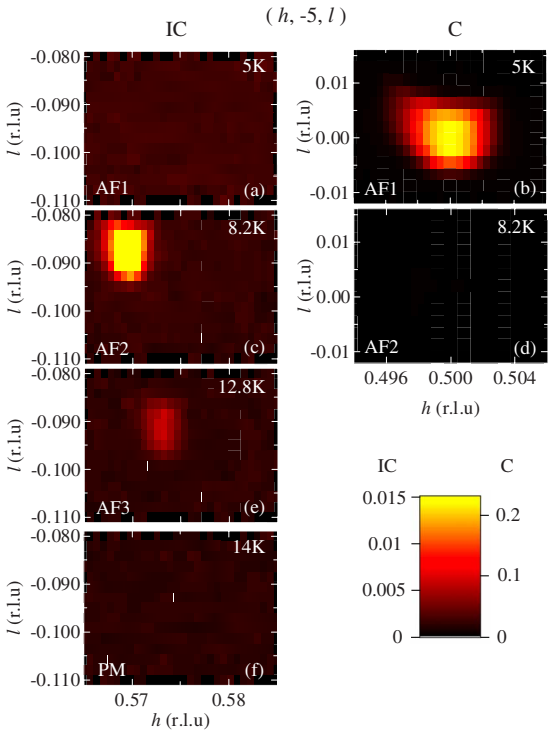

FIG. 2. (Color online) Intensity contour map of IC and C superlattice peaks observed by the synchrotron x-ray diffraction measurements in the $(h,-5,l)$ zone with $h\sim 1/2$, $l\sim 0$. [(a) and (b)] 5 K (AF1), [(c) and (d)] 8.2 K (AF2), (e) 12.8 K (AF3), and (f) 14 K [paramagnetic (PM) phase]. Data were collected in a warming process.

electric polarization P, gold electrodes were sputtered onto the opposite faces of the samples. The crystals with the gold electrodes were annealed at 500 °C for 1 h. We obtained P by integration of pyroelectric or magnetoelectric current, which was measured with an electrometer (Keithley 6517A) applying an electric field of 500 kV/m [except for the data shown in Fig. 3(d)]. The measurements of P in a magnetic field up to 14.5 T were performed at the High Field Laboratory for Superconducting Materials, Institute for Materials Research, Tohoku University, Japan. We applied magnetic fields along one of the two crystallographic principal axes, the *a* or the *c* axis, or the magnetic easy axis, which forms an angle of 35° with the *a* axis in the *ac* plane. Magnetization was measured by a commercial superconducting quantum interference device magnetometer.

III. RESULTS AND DISCUSSION

A. Spin-lattice coupling at zero magnetic field

Figure 2 shows contour maps of C and IC superlattice peak intensities around $\boldsymbol{Q}=(h,-5,l)$ with $h\sim 1/2$, $l\sim 0$ in each magnetic phase. An intense C superlattice peak is discernible in the AF1 phase, whereas an IC superlattice peak is observed in the AF2 and AF3 phases. The emergence of the C and IC lattice modulation seems to correspond to the magnetic modulation, since the lattice propagation vector ($\boldsymbol{q}^l$) of

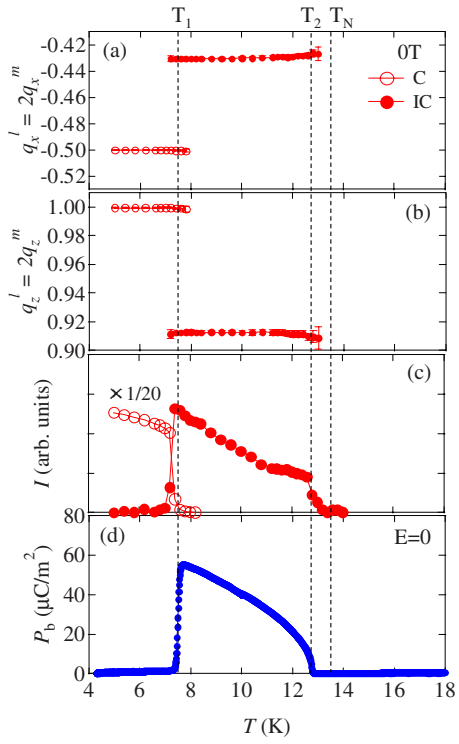

FIG. 3. (Color online) Temperature dependences of [(a) and (b)] lattice propagation vectors q_x^l and q_z^l, (c) integrated intensities of IC (closed circles), C (open circles) superlattice peaks, and (d) electric polarization along the b axis (P_b) at 0 T. P_b was obtained by integrating the pyroelectric current with respect to time. The pyroelectric current measurements were performed after poling the crystals (500 kV/m) during the cooling process from a temperature above the Néel temperature down to 10 K. Before measurements, the poling electric field was removed.

each phase is almost twice the magnetic propagation vector ($\boldsymbol{q}^m$) obtained from a neutron diffraction measurement.[20] This relationship between $\boldsymbol{q}^l$ and $\boldsymbol{q}^m$, $\boldsymbol{q}^l=2\boldsymbol{q}^m$, is also reported in many other multiferroic materials[1,13,21] and indicates that the magnetic modulation induces the lattice modulation through the spin-lattice coupling termed exchange striction. Comparing Figs. 2(c) and 2(e), the position of superlattice peaks are slightly different between AF2 (8.2 K) and AF3 (12.8 K). The $\boldsymbol{q}^l$ values of the two phases are (−0.430,0,0.912) and (−0.426,0,0.909), respectively. This result is consistent with a previous neutron diffraction measurement of a single crystal.[22] The temperature dependence of the superlattice propagation vector $\boldsymbol{q}^l$ is shown in Figs. 3(a) and 3(b). The x and z components of the lattice propagation vector, q_x^l and q_z^l, continuously shift from the AF3 to the AF2 phase around T_2, whereas q_x^l and q_z^l discontinuously change to C values, $q_x^l=-0.5$ and $q_z^l=1$, around the ICM-CM transition temperature (T_1) from the AF2 to the AF1 phase. This ICM-CM transition is known to be of first order.[20] Figure 3(c) shows the temperature dependence of the integrated intensities for the C and IC superlattice peaks, $(1+q_x^l,-5,-1+q_z^l)$. The IC peak gradually grows in intensity below T_N until the development of the superlattice peak intensity is suppressed below T_2. The coexistence of C and IC superlattice peaks is observed between 7.2 and 7.8 K. The observed two phase coexistence corresponds to the fact that the magnetic phase transition between the AF1 and the AF2 at T_1 is of a first-order type. In the following, we consider the correlation between the exchange striction and the temperature dependence of the IC peak intensity in the AF2 and AF3 phases. In these phases, the spin $\boldsymbol{S}_i$ on the ith Mn site is described as

$$\boldsymbol{S}_i = \boldsymbol{S}_{easy}\cos(2\pi\boldsymbol{q}^m\cdot\boldsymbol{R}_i) + \boldsymbol{S}_b\sin(2\pi\boldsymbol{q}^m\cdot\boldsymbol{R}_i). \quad (2)$$

Here, $\boldsymbol{S}_{easy}$ and $\boldsymbol{S}_b$ are the spin components parallel to the magnetic easy and crystallographic b axis, respectively. $\boldsymbol{R}_i$ represents the ith Mn site position. The magnetic structure in each phase is described by introducing the ellipticity, which is defined as $\eta=S_b/S_{easy}$. In the spiral phase (AF2), η has a nonzero value, whereas $\eta=0$ in the sinusoidal phase (AF3). In both phases, the exchange striction, which is proportional to $\boldsymbol{S}_i\cdot\boldsymbol{S}_{i+1}$, induces the lattice modulation. Since the $2\boldsymbol{q}^m$ component of $\boldsymbol{S}_i\cdot\boldsymbol{S}_{i+1}$ is proportional to $S_{easy}^2(1-\eta^2)$ in the magnetic structure described by Eq. (2) and S_{easy} develops in the cooling process, the suppression of the peak intensity development below T_2 would be ascribed to the suppression of the lattice modulation caused by the fact that $\eta\neq 0$ in the AF2 phase. A similar phenomenon is also observed in the x-ray diffraction measurements of $TbMnO_3$.[1] As shown in Figs. 3(c) and 3(d), both the IC peak intensity and the electric polarization increase in the cooling process. Since the magnetic propagation vector $\boldsymbol{q}^m$ hardly changes, as shown in Figs. 3(a) and 3(b), the electric polarization deduced from Eq. (1) in the spiral-spin structure described by Eq. (2) is proportional to $S_{easy}^2\eta$. For the simultaneous increase of both the IC peak intensity and the electric polarization in the spiral-spin phase, as observed in Figs. 3(c) and 3(d), S_{easy} alone should develop with an almost constant ellipticity η. This scenario has recently been confirmed by a spin-polarized neutron diffraction study.[23]

B. Magnetic-field-induced phase transition in $H\|$easy axis

Figures 4(a) and 4(b) display the temperature dependence of P_b, which is the electric polarization parallel to the b axis, in several magnetic fields parallel to the easy axis ($\boldsymbol{u}$). For the magnetic field between 3 and 12 T, the P_b gradually grows down to the lowest temperature, as reported in the previous research.[24] The disappearance of the paraelectric AF1 phase indicates the stabilization of the AF2 phase by the application of magnetic field parallel to $\boldsymbol{u}$, along which the spins antiferromagnetically align in the collinear AF1 and AF3 phases. This behavior can be easily understood because the magnetic field along $\boldsymbol{u}$ tends to induce the [010] component of spin, which is perpendicular to $\boldsymbol{u}$. We can also confirm the slight decrease of P_b above 3 T, which has been previously reported.[24] In Fig. 4(b), we show the P_b behavior in the high magnetic fields up to 14.5 T. The FE polarization along the b axis disappears again above 13 T in the low temperature range. The temperature range for the FE AF2 phase becomes narrower with increasing the applied magnetic field. Some new phase is stabilized by magnetic fields along $\boldsymbol{u}$ higher than 13 T. The observed new phase without

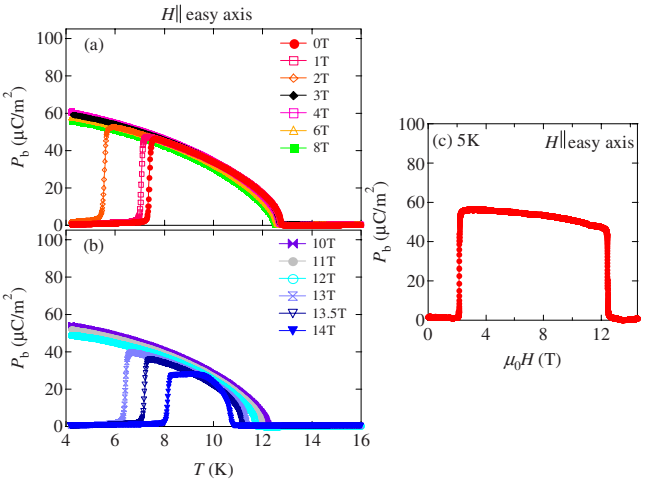

FIG. 4. (Color online) [(a) and (b)] Temperature dependence of electric polarization along the b axis (P_b) in several magnetic fields along the easy axis. P_b (a) for 3, 4, 6, and 8 T in almost overlap, (b) as well as that for 10, 11, and 12 T. (c) Magnetic-field-induced change in P_b as a function of an external magnetic field parallel to the easy axis at 5 K.

FE polarization along the b axis should correspond to the HF phase previously reported based on a magnetization measurement.[22] Since this HF phase merges into the AF1 phase when the magnetic field is applied to the intermediate direction between the b axis and $\boldsymbol{u}$, the same translational symmetry for both phases is suggested in Ref. 22. This fact indicates that the HF phase would also be a nonpolar one, as well as the AF1 phase, in which the FE polarization disappears. In Fig. 4(c), we display the magnetic field ($H\|\boldsymbol{u}$) dependence of P_b in an H-increasing process at 5 K. Around 2.1 T, P_b increases steeply. The appearance of P_b corresponds to the phase transition from the AF1 to the spiral AF2 phase. With further increasing H, P_b is suddenly suppressed around 12.4 T. This suppression agrees with the phase transition from the AF2 to the HF phase. Speculating from the fact that the FE phase appears only in the spiral-spin phase in $MnWO_4$, the magnetic structure of the HF phase would be a spin canted structure along $\boldsymbol{u}$, which would correspond to the spin-flopped state of the AF1 phase. The speculated spin canted state is also consistent with the fact that the HF phase merges into the AF1 phase for the magnetic field, which forms the angle of about 45° with $\boldsymbol{u}$ in the plane spanned by the b axis and $\boldsymbol{u}$.[22] In this magnetic-field direction, the spin canted AF1 and HF structures would coincide. In accordance with the discontinuous jump of P_b, a hysteretic behavior is observed around the boundary between the AF2 and HF phases.

We summarize the magnetoelectric phase diagram for the magnetic field along the easy axis ($\boldsymbol{u}$) in Fig. 5. Closed and open squares represent the data points obtained from pyroelectric or magnetoelectric current measurements in the cooling (or H decreasing) and warming (or H increasing) runs, respectively. The magnetic phase boundary between the AF3 and paramagnetic phases is also represented by the closed triangles (excerpts from Ref. 24). This phase diagram is very similar to the magnetic phase diagram reported by Ehrenberg

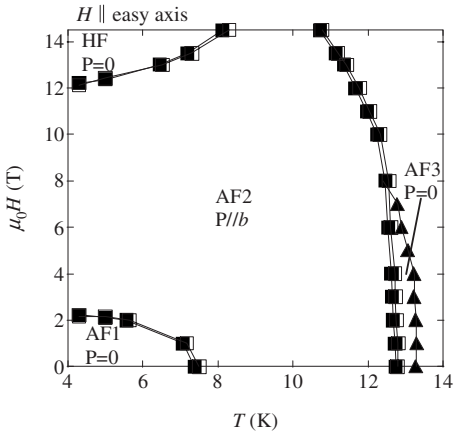

FIG. 5. Magnetoelectric phase diagram in magnetic fields parallel to the easy axis ($\boldsymbol{u}$). Closed and open squares represent the data points in the cooling (or H decreasing) and warming (or H increasing) runs of pyroelectric and magnetoelectric current measurements, respectively. Closed triangles show magnetic phase transition temperatures (excerpts from Ref. 24).

et al.[22] Here, we can reconfirm that the FE polarization appears only in the AF2 phase but not in the HF phase.

C. Magnetic-field-induced phase transition in $H\|a$ and c

In Figs. 6(a) and 6(b), we display the temperature dependence of P_b in several magnetic fields applied parallel to the a and c axes, respectively. In both cases, the temperature range, where nonzero P_b appears, becomes broader as the magnetic field increases. When the magnetic field higher than 3 T (4 T) is applied along the a (c) axis, the FE phase is stabilized down to the lowest temperature, ~4.2 K. The

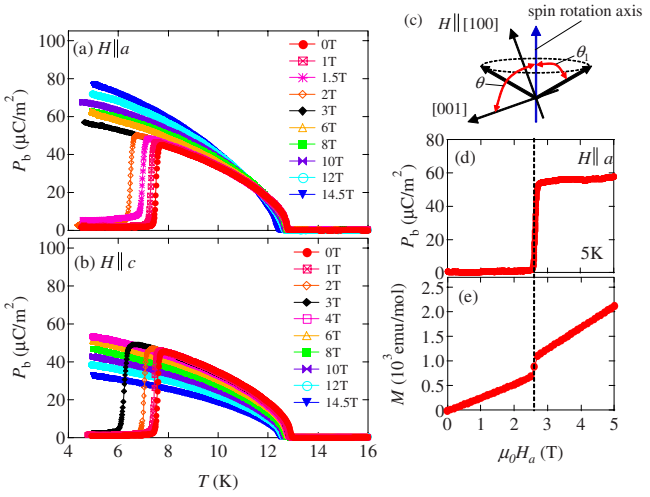

FIG. 6. (Color online) [(a) and (b)] Temperature dependence of electric polarization along the b axis (P_b) in several magnetic fields along the a and c axes. (c) Schematic drawing of the conical structure in the magnetic field parallel to the a axis. The spin rotation axis is also displayed. (d) Magnetic-field-induced change in P_b as a function of an external magnetic field parallel to the a axis. (e) Magnetic-field dependence of the magnetization along the a axis at 5 K.

magnetic field along the a or the c axis stabilizes the spiral-spin structure with ferroelectricity as in $H\|$easy axis. In Figs. 6(d) and 6(e), the magnetic-field ($H\|a$) dependence of P_b and that of magnetization (M) are shown, respectively. As magnetization shows a jump upon the phase transition from AF1 to AF2 at around 2.6 T, P_b appears. The same behavior is also observed in the $H\|c$ case (not shown). This simultaneous FE phase transition with the magnetic transition again confirms that the FE phase coincides with the AF2 phase with spiral-spin structure.

The magnetic-field dependence of P_b in $H\|a$ and $H\|c$ shows a contrasting behavior. As displayed in Figs. 6(a) and 6(b), P_b increases in $H\|a$ ($dP/dH_a>0$), whereas it decreases in $H\|c$ ($dP/dH_c<0$). When the magnetic field is applied parallel to the a or the c axis, a ferromagnetic component is appended to the spiral structure. We approximately regard this magnetic structure as conical, as shown in Fig. 6(c). In the conical structure, spin $\boldsymbol{S}_i$ on the ith Mn site is described as

$$\boldsymbol{S}_i = S\sin\theta_1\cos(2\pi\boldsymbol{q}^m\cdot\boldsymbol{R}_i)\boldsymbol{u}_1 + S\sin\theta_1\sin(2\pi\boldsymbol{q}^m\cdot\boldsymbol{R}_i)\boldsymbol{u}_2 + S\cos\theta_1\boldsymbol{u}_3. \quad (3)$$

$\boldsymbol{u}_i$ ($i=1,2,3$) is the orthogonal unit vector. $\boldsymbol{u}_3$ is directed to the spin rotation axis of the conical structure, and $\boldsymbol{u}_2$ is parallel to the crystallographic b axis. θ_1 represents the cone angle in the conical spin state. S is the spin amplitude. In the following, we consider the simple situation at low temperatures, where S fully develops and is regarded as a constant value. Taking into account that the Mn^{2+} one-dimensional chain is along the c axis, the predicted P_b from Eq. (3) in the conical state is proportional to $\sin\theta\sin^2\theta_1\sin(\pi q_z^m)$. Here, the parameter θ represents the angle between the crystallographic c axis and the spin rotation axis. As shown in Figs. 7(a) and 7(b), the lattice modulation shows little change in the ICM-AF2 phase in the magnetic field. Since this behavior indicates that the magnetic field hardly affects the z component of the magnetic propagation vector (q_z^m), P_b would be approximately proportional to $\sin\theta\sin^2\theta_1$. In both cases in $H\|a$ and $H\|c$, $\sin^2\theta_1$ decreases as the conical umbrella structure is closed by the applied magnetic fields. Therefore, the contrasting behaviors of P_b in $H\|a$ and $H\|c$ should be dominated by the parameter θ. In $H\|a$ and $H\|c$, the spin rotation axis would approach the applied magnetic-field direction and finally become parallel. θ approaches $\sim 90°$ in $H\|a$, whereas it approaches 0° in $H\|c$. As a result, P_b increases in $H\|a$, while it decreases in $H\|c$. This prediction based on a simple model is qualitatively consistent with the contrasting behavior of P_b shown in Figs. 6(a) and 6(b).

In Fig. 7, we compare the magnetic-field dependence of the superlattice reflection with that of P_b in $H\|c$ at 6 K. The integrated intensities of the superlattice peak is displayed in Fig. 7(c). Around 3 T, where the magnetic field induces FE phase transition [Fig. 7(d)], the C-IC phase transition, which corresponds to the phase transition from AF1 to AF2, is observed, as shown in Figs. 7(a)–7(c). We can confirm that the FE AF2 phase in a magnetic field also takes the incommensurate magnetic structure. In addition, the two phase coexistence, which reflects the first-order-type magnetic phase transition from AF1 to AF2, is also confirmed at 3 T [Fig. 7(c)]. As shown in Fig. 7(c), the intensity of the superlattice peak decreases with increasing magnetic field as well as the electric polarization in the AF2 phase. As discussed in Sec. III A, the simultaneous decrease of the peak intensity and the electric polarization can be attributed to the decrease of $S\sin\theta_1$, which is the amplitude of the spin component perpendicular to the spin rotation axis in the magnetic field parallel to the c axis.

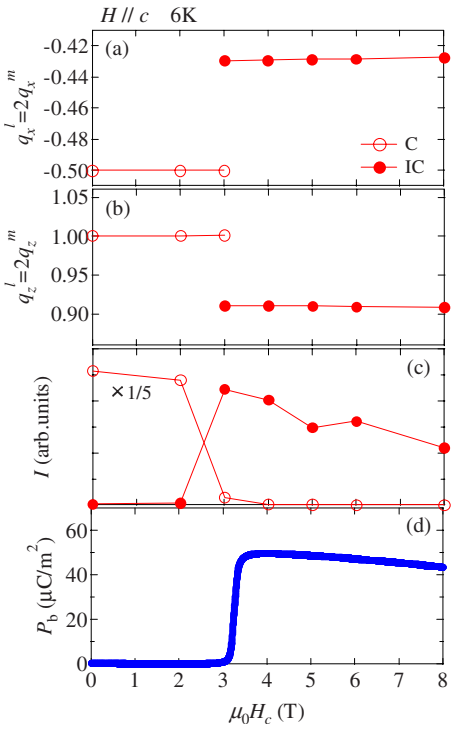

FIG. 7. (Color online) Magnetic-field dependences of [(a) and (b)] lattice propagation vectors q_x^l and q_z^l, (c) integrated intensities of IC (closed circles), C (open circles) superlattice peaks, and (d) electric polarization along the b axis (P_b) at 6 K. The magnetic field is applied along the c axis.

Figures 8(a) and 8(b) show the magnetoelectric phase diagrams for the magnetic-field direction along the a and the c axis, respectively. Closed and open squares represent the data points obtained from pyroelectric and magnetoelectric current measurements in the cooling (or H decreasing) and warming (or H increasing) runs, respectively. Hysteresis is observed at the boundary between AF1 and AF2, reflecting the first-order-like change of the electric polarization. The phase diagrams in Figs. 8(a) and 8(b) resemble the magnetoelectric phase diagram in $H\|$easy axis shown in Fig. 5. Since the magnetic principal axes in the ac plane are not identical with the crystallographic axes, as shown in Fig. 1(b), the applied magnetic field along the crystallographic axis, which is the a or the c axis, is decomposed to the two components, H_u and H_v, which are the easy axis and the hard axis components of the magnetic field, respectively. Taking into account that the H_u component stabilizes the FE AF2 phase and the H_v component stabilizes the nonpolar AF1 phase,[22,24] the phase diagrams shown in Fig. 8 indicate that the magnetic-field component along the easy axis (H_u) is

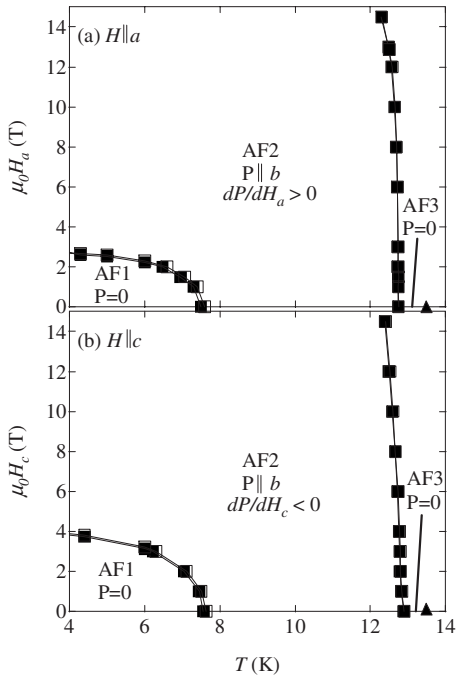

FIG. 8. Magnetoelectric phase diagram in magnetic fields parallel to (a) the *a* axis and (b) the *c* axis. Closed and open squares represent the data points in the cooling (or *H* decreasing) and warming (or *H* increasing) runs of pyroelectric and magnetoelectric current measurements, respectively. Closed triangles show the magnetic phase transition temperature, determined by the magnetic susceptibility measurements in a cooling run.

more dominant than that of the hard axis (H_v) for both cases in $H\|a$ and $H\|c$. Comparing the phase diagram in Fig. 8(a) with that in Fig. 8(b), the transition magnetic fields from AF1 to AF2 are smaller in $H\|a$ than in $H\|c$. This difference can be explained by the relative configuration of the *a*, *c*, and easy axes. Since the *a* axis is closer to the magnetic easy axis than the *c* axis, the easy axis component is larger in $H\|a$ than in $H\|c$.

IV. CONCLUSION

In summary, we have investigated the magnetic-field dependence of the FE phase and the spin-lattice coupling in $MnWO_4$. The HF phase, which appears when the magnetic field is applied along the easy axis, turned out to be a nonpolar phase. From this electric property, we can deduce the magnetic structure in the HF phase as a canted spin 1 through the magnetoelectric relationship. It has been observed that the magnetic fields parallel to the *a* or the *c* axis also induce FE phase transition. This means that the easy axis component of the magnetic field is more dominant than the hard axis one in the *ac* plane, since the easy axis component of the magnetic field alone stabilizes the FE AF2 phase. The contrasting magnetic-field dependence of the FE polarization for $H\|a$ and $H\|c$ seems to be explained qualitatively by taking into account the relative configuration between the crystallographic axes and the magnetic principal axes in the *ac* plane. We have also confirmed that the AF2 phase accompanies the IC lattice modulation regardless of the magnetic field. This fact indicates that the magnetic-field-induced AF2 phase also takes the ICM structure.

ACKNOWLEDGMENTS

We thank M. Saito for help with experiments. This work was partly supported by Grants-In-Aid for Scientific Research (No. 19740190, No. 16076207, and No. 19052001) from the MEXT, Japan.

[1] T. Kimura, T. Goto, H. Shintani, K. Ishizaka, T. Arima, and Y. Tokura, Nature (London) **426**, 55 (2003).
[2] N. Hur, S. Park, P. A. Sharma, J. S. Ahn, S. Guha, and S.-W. Cheong, Nature (London) **429**, 392 (2004).
[3] T. Goto, T. Kimura, G. Lawes, A. P. Ramirez, and Y. Tokura, Phys. Rev. Lett. **92**, 257201 (2004).
[4] G. Lawes, A. B. Harris, T. Kimura, N. Rogado, R. J. Cava, A. Aharony, O. Entin-Wohlman, T. Yildrim, M. Kenzelmann, C. Broholm, and A. P. Ramirez, Phys. Rev. Lett. **95**, 087205 (2005).
[5] Y. Yamasaki, S. Miyasaka, Y. Kaneko, J.-P. He, T. Arima, and Y. Tokura, Phys. Rev. Lett. **96**, 207204 (2006).
[6] K. Taniguchi, N. Abe, T. Takenobu, Y. Iwasa, and T. Arima, Phys. Rev. Lett. **97**, 097203 (2006).
[7] S. Park, Y. J. Choi, C. L. Zhang, and S.-W. Cheong, Phys. Rev. Lett. **98**, 057601 (2007).
[8] Y. Naito, K. Sato, Y. Yasui, Y. Kobayashi, Y. Kobayashi, and M. Sato, J. Phys. Soc. Jpn. **76**, 023708 (2007).
[9] T. Kimura, G. Lawes, and A. P. Ramirez, Phys. Rev. Lett. **94**, 137201 (2005).
[10] T. Kimura, J. C. Lashley, and A. P. Ramirez, Phys. Rev. B **73**, 220401(R) (2006).
[11] M. Kenzelmann, G. Lawes, A. B. Harris, G. Gasparovic, C. Broholm, A. P. Ramirez, G. A. Jorge, M. Jaime, S. Park, Q. Huang, A. Ya. Shapiro, and L. A. Demianets, Phys. Rev. Lett. **98**, 267205 (2007).
[12] M. Kenzelmann, A. B. Harris, S. Jonas, C. Broholm, J. Schefer, S. B. Kim, C. L. Zhang, S.-W. Cheong, O. P. Vajk, and J. W. Lynn, Phys. Rev. Lett. **95**, 087206 (2005).
[13] T. Arima, A. Tokunaga, T. Goto, H. Kimura, Y. Noda, and Y. Tokura, Phys. Rev. Lett. **96**, 097202 (2006).
[14] H. Katsura, N. Nagaosa, and A. V. Balatsky, Phys. Rev. Lett. **95**, 057205 (2005).
[15] M. Mostovoy, Phys. Rev. Lett. **96**, 067601 (2006).
[16] I. A. Sergienko and E. D. Dagotto, Phys. Rev. B **73**, 094434 (2006).
[17] A. W. Sleight, Acta Crystallogr., Sect. B: Struct. Crystallogr. Cryst. Chem. **28**, 2899 (1972).
[18] H. Weitzel, Neues Jahrb. Mineral., Abh. **113**, 13 (1970).
[19] H. Dachs, Solid State Commun. **7**, 1015 (1969).
[20] G. Lautenschläger, H. Weitzel, T. Vogt, R. Hock, A. Böhm, M. Bonnet, and H. Fuess, Phys. Rev. B **48**, 6087 (1993).

[21] D. Higashiyama, S. Miyasaka, N. Kida, T. Arima, and Y. Tokura, Phys. Rev. B **70**, 174405 (2004).

[22] H. Ehrenberg, H. Weitzel, C. Heid, H. Fuess, G. Wltschek, T. Kroener, J. van Tol, and M. Bonnet, J. Phys.: Condens. Matter **9**, 3189 (1997).

[23] H. Sagayama, K. Taniguchi, N. Abe, T. Arima, M. Soda, M. Matsuura, and K. Hirota (unpublished).

[24] A. H. Arkenbout, T. T. M. Palstra, T. Siegrist, and T. Kimura, Phys. Rev. B **74**, 184431 (2006).